Innovative Food Science and Emerging Technologies 76 (2022) 102932

Contents lists available at ScienceDirect

Innovative Food Science and Emerging Technologies

journal homepage: www.elsevier.com/locate/ifset

Applying ultrasound-assisted processing to obtain cellulose fibres from rice straw to be used as reinforcing agents

Pedro A.V. Freitas *, Chelo González-Martínez, Amparo Chiralt

Institute of Food Engineering for Development, Universitat Politècnica de València, 46022 Valencia, Spain

ARTICLE INFO

Keywords:
Green method
Ultrasound-heating method
Agro-industrial waste
Cellulose microfibrils
Reinforcing capacity
Methylcellulose

ABSTRACT

Rice straw (RS) is one of the most globally abundant agro-industrial residues. For its valorisation, a green combined ultrasound-reflux heating method was applied to obtain cellulose fibres (CF) from RS. The new method produced CF with a higher yield (37%) than the alkaline process (29%), more hydrophilic, and with a lower tendency to aggregate. Despite the slightly different degree of purification detected by the chemical and FTIR analysis, both fibres exhibited similar crystallinity, thermal behaviour, morphogeometric characteristics, and aspect ratio distributions (20–60). Both CF showed similar reinforcing capabilities in methylcellulose/gum Arabic films, enhancing the film stretchability and resistance to break by about 33% and 20%. Non-noticeable changes in water vapour permeability and the light internal transmission were observed, indicating good compatibility CF-polymer matrix. Therefore, using the ultrasound-heating method to obtain CF is an eco-friendlier process than the alkaline treatment, supplying suitable fibres as industrial reinforcing agents.

Industrial relevance: Ultrasound, an emerging technology in food processing, combined with reflux heating, can be a green alternative for obtaining cellulose microfibres for industrial applications. The new combined method was faster than the alkaline process (1.5 h *vs.* 6 h) and was more environmentally-friendly since it does not require a strong alkaline solution. Besides, both cellulose microfibres exhibited similar performances when incorporated into a polymer matrix. These results boost knowledge in the food packaging field, as well as the valorisation of agro-industrial wastes for industrial applications.

1. Introduction

Agricultural residues generated as wastes during or after the processing of agricultural crops are one example of a renewable resource that is available in huge amounts. Many of these agricultural residues are lignocellulose-rich, primarily containing cellulose, lignin, hemicellulose, and extractives, such as phenolic compounds (Saini, Saini, & Tewari, 2015). So, the agro-industrial waste derivatives could be used as value-added materials with antioxidant and antimicrobial properties (Freitas, González-Martínez, & Chiralt, 2020; Menzel, González-Martínez, Vilaplana, Diretto, & Chiralt, 2020; Prakash et al., 2018), biomass for fuel production (Casabar, Ramaraj, Tipnee, & Unpaprom, 2020; Takano & Hoshino, 2018) or reinforcing fillers in polymeric materials useful in food packaging. The application of lignocellulosic agro-wastes in food packaging manufacturing processes is highly promising since these are renewable materials and their use contributes to boosting the management and valorisation of agro-industrial waste in the context of the circular economy (Collazo-Bigliardi, Ortega-Toro, & Chiralt, 2019; Freitas et al., 2020; Ng et al., 2015a; Sharma et al., 2019). Many studies have reported the isolation of different cellulose fractions from lignocellulosic by-products for different purposes. Residues, such as walnut shell, corncob and sugarcane bagasse (Harini & Chandra Mohan, 2020), pea and broad beans (Kassab, 2020), sugar palm (Ilyas et al., 2019), sugarcane bagasse (Saha & Ghosh, 2019), coffee and rice husk (Collazo-Bigliardi, 2018; Kargarzadeh, 2017; Requena et al., 2019) and rice straw (RS) (Boonterm, 2016), have been characterised as to their cellulose content and extraction.

Rice (*Oryza sativa* L.) is one of the most important global crops, with an annual world production of 780 million tons, which generates a large amount of RS (FAOSTAT, 2018; Peanparkdee & Iwamoto, 2019). RS, the leftover from rice production that includes stems, leaf blades, leaf sheaths, and the remains of the panicle after threshing, is one of the most abundant lignocellulosic waste materials in the world (Saini et al., 2015). After harvesting, the RS by-product is usually burned in the fields, which causes environmental and health problems in the population living near the rice paddies (Peanparkdee & Iwamoto, 2019; Sarkar,

* Corresponding author.
E-mail address: pedroafreitas3@gmail.com (P.A.V. Freitas).

https://doi.org/10.1016/j.ifset.2022.102932
Received 26 May 2021; Received in revised form 10 December 2021; Accepted 8 January 2022
Available online 13 January 2022

Ghosh, Bannerjee, & Aikat, 2012). Considering that the lignocellulosic fraction represents approximately 70% of the RS dry matter (Barana, Salanti, Orlandi, Ali, & Zoia, 2016), taking advantage of the cellulosic derivatives from this residual biomass is of great interest, as is their use as reinforcing agents in polymeric materials. Numerous studies can be found using nanocellulose (crystals of fibres) from different sources as reinforcement agents. In particular, micro or nanocrystals (CNC) from RS have been incorporated into different polymeric matrices, such as polyvinyl alcohol (PVA) (Ching, Rahman, Ching, Sukiman, & Cheng, 2015), or cellulose acetate (Hassan et al., 2019). Nevertheless, few studies reported the use of cellulose fibres (CF). The use of CF instead of nanocrystals presents some advantages, such as a higher cellulose yield and a greater strength and elastic modulus, due to the higher aspect ratio of CF and fibre entanglements (Xu, 2013). The fibre entanglements play an important role in the force transferring from matrix to fibrils and from fibrils to fibrils.

The lignocellulosic fraction of RS consists of a complex matrix assembled by semicrystalline cellulose microfibrils, as the primary fibre component, linked to a cementing matrix composed of hemicellulose and lignin (Chen, 2011). Separating cellulose into its elemental form of nanofibrils, approximately 3–20 nm in width, is a difficult task. Among the chemical and physical treatments for obtaining cellulose fibres, the most common method focuses on treating biomass with a strongly alkaline sodium hydroxide solution. This alkaline treatment, also known as mercerisation, promotes the degradation of a substantial fraction of hemicellulose, lignin, and waxes present in the cellulosic material (Boonterm, 2016; Zhang, Smith, & Li, 2014). However, the alkaline treatment is associated with environmental problems due to the large amounts of contaminant alkaline solvent used and the need for a large quantity of water with which to wash the material after the extraction process (Boonterm, 2016). Moreover, the highly alkaline environment can induce the formation of stable bonds between hemicellulose and lignin, limiting the biomass delignification step (Salam, Reddy, & Yang, 2007). In this sense, some studies have been conducted to eliminate alkaline treatment in the cellulose purification, using steam explosion technique (Wang, 2018). Other more environmentally-friendly alternative treatments, such as combined ultrasound and heating processes, could also be used to replace the alkaline treatment in the extraction of hemicellulose and lignin from biomass. This combined process has been previously applied to obtain active extracts from RS with high extraction yield and antioxidant activity (Freitas et al., 2020). Being the extraction residue rich in cellulosic components, it has a great potential to be used as a source of cellulose fibres since it has been partially purified. Likewise, the US treated plant tissue could be more easily bleached due to the structural alterations provoked by the combined extraction process. In this sense, an integral process consisting of extraction of active compounds and obtaining cellulose fibres could be designed for a better valorisation of RS.

Ultrasound-assisted extraction (UAE) is an emerging, green operation that applies intense mechanical shear forces in a plant matrix to disrupt its primary structure and leach out target compounds (Cheung & Wu, 2013). The high shear rates stem from acoustic cavitation, a physical phenomenon characterised by the collapse of air or water vapour bubbles formed by the compression and rarefaction of ultrasonic waves propagating in the solvent (Ojha, 2020; Sumere et al., 2018). Likewise, another eco-friendly technique to extract compounds from lignocellulosic matrices is the heating of the aqueous dispersion of ground plant matrix at high temperatures (above 100 °C) (Wanyo, Meeso, & Siriamornpun, 2014). This promotes the cleavage of covalent bonds and Van der Waals forces present in the lignocellulosic fraction, extracting, or degrading, part of the hemicellulose, lignin, and other components (Korotkova et al., 2015). To enhance the water extraction efficiency of RS compounds, Freitas et al. (2020) applied ultrasound (US) as pre-treatment, followed by a reflux heating step. The extracts obtained by using US pre-treatment had the highest levels of phenolic compounds and total solid content, due to the greater extraction of hemicellulose and lignin fractions. To the best of our knowledge, the combined ultrasound-reflux heating method has not yet been used as a step for obtaining cellulose fibres from RS.

Of the potential applications of cellulosic fibres, their reinforcing capacity may improve the functional properties of films aimed to food packaging. In this sense, Methylcellulose (MC), a biopolymer derived from cellulose, composed of methyl substitution groups linked to the native cellulose backbone (Nunes et al., 2018), is a biodegradable, non-toxic, with good adhesiveness, biocompatibility, and mechanical properties, with promising potential to be used as a food packaging material (Saha & Ghosh, 2019). Incorporation of cellulose fibre in this polymer matrix may improve its performance as packaging material. Likewise, the incorporation of other components such as gum Arabic (GA), a polysaccharide-protein complex, which can act as compatibilizer (Amalraj, Haponiuk, Thomas, & Gopi, 2020; Xu et al., 2018), could improve the fibre function in the film, promoting the reinforcing effect.

Therefore, the aim of this study was to obtain cellulose fibres (CF) from RS by applying the combined ultrasound-heating method plus a bleaching step. Ultrasounds were also applied to disaggregate fibre bundles in water medium and the fibrils were tested as reinforcing agents in Methylcellulose/Gum Arabic blend films. CF were characterised as to their different nano and microstructural characteristics, thermal behaviour and reinforcing capacity and compared with those obtained by applying the conventional alkaline treatment.

2. Material and methods

2.1. Plant material and chemicals

RS (*O. sativa* L. var. *J. Sendra*) was collected in a L'Albufera paddy field (Valencia, Spain), dried (50 ± 2 °C, 0.5 mmbar for 16 h), milled (3 cycles of 90 s each) using a grinding machine (IKA, model M20, Germany), and sieved to achieve particle sizes of under 0.5 mm. Methylcellulose (MC: viscosity of 15 cP), gum Arabic (GA), sodium chlorite, and sodium hydroxide were supplied by Sigma-Aldrich (United States). Glycerol, acetic acid, magnesium nitrate ($Mg(NO_3)_2$), and phosphorus pentoxide (P_2O_5) were purchased from Panreac Química (Spain). Sodium acetate trihydrate was supplied by FlukaTM (Germany).

2.2. Purification treatments of the cellulosic fraction from RS

2.2.1. Combined ultrasound-heating treatment

An alternative treatment based on a consecutive combination of ultrasound and heating was applied to extract hemicellulose and lignin fractions from RS. Firstly, a RS aqueous dispersion (5%, *w/v*) was sonicated for 30 min with a probe-type high-intensity ultrasonic homogenizer (Vibra Cell™ VCX750, Sonics & Material, United States), using 750 W power, 20 kHz frequency, and 40% sonication amplitude. During sonication, sample was immersed in an ice bath to control the temperature that raised from 25 to 40 °C. The total ultrasonic power applied to the extraction system was calculated according to the calorimetric method (Kimura et al., 1996), with some modifications. To this end, the temperature increases of the system containing water was recorded every minute, by duplicate, and the applied acoustic power was calculated from the slope of the temperature-time curve. The obtained value was 31 ± 3 W, lower than the electric power of the equipment (750 W).

After sonication, the dispersion was heated at reflux temperature (100 °C) for 1 h, filtered and washed several times with distilled water to eliminate water soluble extract retained in the solid. The insoluble fraction from the combined (RUH) method was dried at 35 ± 2 °C for 48 h.

2.2.2. Alkali treatment

The alkali treatment was carried out following that described by Collazo-Bigliardi (2018), using an RS: sodium hydroxide solution (4.5%, *w/v*) at a ratio of 1:20 (*w/v*). The plant dispersion was heated at reflux

temperature (100 °C) for 3 h. Afterwards, the insoluble material (RALK) was filtered, washed with distilled water until neutral pH to eliminate the alkali solution, and dried at 35 ± 2 °C for 48 h. Three RS samples were treated with alkaline solution twice.

2.2.3. Bleaching treatment

The samples obtained from those previously described treatments were bleached, following Requena et al. (2019), with some modifications. The bleaching solution was obtained by mixing equal parts of distilled water, acetate buffer solution (2 N), and sodium chlorite (1.7%, *w/v*). Thus, the cellulosic material was mixed with the bleaching solution (5%, w/v) and heated at reflux for 4 h. Afterwards, the dispersion was filtered and washed with distilled water until the complete removal of bleach solution residues. The bleached materials (RALK-B and RUH-B) were dried at 35 °C for 24 h. For each cellulosic sample, the bleaching process was performed four times while the process was repeated three times on different samples.

2.3. Characterisation of CF from RS

2.3.1. Moisture content

The equilibrium moisture content of cellulosic fractions was determined gravimetrically. Approximately 1.5–3 g of each cellulosic fraction was conditioned at 25 °C and different relative humidity (RH), in desiccators with different salt saturated solutions ($MgCl_2$: 53%; NaCl: 75%; and KCl: 84%) for two weeks and then were dried at 60 °C for 24 h. Afterwards, the samples were placed in a desiccator at 25 °C with P_2O_5 for two weeks. The moisture contents were determined from the total weight loss of the conditioned samples and expressed as percentage on dry basis. The analysis was performed in triplicate for each treatment. Samples of RS were conditioned at 53% RH before their use and the equilibrium moisture content (5.1 ± 0.3 g/100 g d.s.) was obtained by the same procedure.

2.3.2. Chemical composition

The cellulose, hemicellulose, and lignin content of the untreated RS and each lignocellulosic fraction was performed according to the standard NREL method (NREL/TP-510-42,618) (Sluiter, 2008b). In brief, the cellulosic materials were subjected to hydrolysis with sulfuric acid, and the lignin content was determined in the insoluble fraction. At the same time, the hydrolysed soluble fractions were used to quantify the sugar composition (typically glucose, xylose, and arabinose) by using high-performance liquid chromatography (HPLC, Agilent Technologies, model 1120 Compact LC, Germany). A HILIC Luna Omega Sugars column (150 × 4.6 mm, 3 μm) and an evaporative light scattering detector (ELSD Agilent Technologies 1200 Series, Germany) were used. The mobile phase was water: acetonitrile (25:75), in isocratic mode, at a flow rate of 0.8 mL.min^{-1}. The detector conditions were: 40 °C, 3.0 bars of gas pressure (N_2), and gain of 3. The software used was ChemStation program (Agilent Technologies, Germany). The cellulose content was expressed as % wt. of glucose in relation to the initial solid fraction, while the hemicellulose concentration was determined by the sum of the xylose and arabinose contents. Before the hydrolyses, the untreated RS and the insoluble fractions after ultrasound (RUS) and reflux heating (RUH) treatments were subject to a water extraction according to the standard NREL method to determine extractives in biomass (NREL/TP-510-42,619) (Sluiter, 2008a). The ash content was determined thermogravimetrically using a thermogravimetric analyser (TGA 1 Stare System, Mettler-Toledo, Switzerland). Samples (3–4 mg) were heated from 25 to 700 °C under nitrogen flow (10 mL.min^{-1}) and a heating rate of 10 °C.min^{-1}. The residual mas was considered as ash content.

2.3.3. Morpho-geometric analyses

Both untreated samples and those obtained in each fibre isolation step were evaluated by using an optical microscope (Optika Microscope B-350, Italy) equipped with a camera (Optikam B2). The samples were prepared at 0.001 mg.mL^{-1}, placed on the glass slide, and observed at 10× and 40× magnification. Bleached fibre dispersions (0.001 mg.mL^{-1}) were sonicated using a probe-type high-intensity ultrasonic homogenizer (Vibra Cell™ VCX750, 750 W power, 20 kHz frequency, Sonics & Material, United States) for 20 min before the microscopic observation.

The morphogeometric characteristics of sonicated CF dispersions were determined by measuring the particle length and width. For each sample, a minimum of 50 measurements were taken using the Optika Vision Lite program. The results were expressed in cumulative distributions for each parameter.

The particle size distributions of the water dispersed (0.001 mg.mL^{-1}) and sonicated bleached samples (0.001 mg.mL^{-1}, 20 min ultrasound) were also analysed by using a laser-diffraction particle size analyser (Mastersizer 3000, Malvern Instruments, UK) operating based on the Mie theory. The refractive and absorption indexes of 1.52 and 0.1, respectively, were considered. The samples were diluted, stirred at 1900 rpm, and fed into the system until an obscuration rate of 10% was achieved. The size distribution plots were obtained using volume fraction of particles vs. size. The measurements were taken in triplicate.

2.3.4. Field emission scanning electron microscopy (FESEM)

The morphological characteristics of the cellulosic materials were analysed by using Field Emission Scanning Electron Microscope (ULTRATM 55, Zeiis, Oxford Instruments, UK). The samples were covered with platinum and the micrographs were obtained at an acceleration voltage of 2.00 kV.

2.3.5. Fourier transform infrared spectroscopy (FTIR)

A FTIR spectrometer (Vertex 80, Bruker AXS GmbH, Karlsruhe, Germany) equipped with microscopic (Hiperion) and attenuated total reflectance accessories was used to evaluate the vibrational profile of the functional groups present in the obtained CF. FTIR spectra were obtained at a resolution of 6 cm^{-1}, in the wavelength range of 4000–650 cm^{-1}, and performing 128 scans for each spectrum. The measurements were taken 5 times for each sample.

2.3.6. X-ray diffraction analysis (XRD)

The X-ray diffraction spectra of the cellulosic samples were obtained with an X-ray diffractometer (AXS/D8 Advance, Bruker, Karlsruhe, Germany) using Kα-Cu radiation (λ: 1.542 Å), 40 kV, 40 mA, step size of 2.0°.min^{-1}, and a 2θ scanning angle between 5° and 40°. The conditioned samples (25 °C and 53% relative humidity (RH)) were spread and compacted to cover the sample holder. For each treatment, the crystallinity index (CI, expressed as a percentage) was determined following the Seagal et al. (1959) method, which relates the maximum intensity of 200 lattice diffraction (I_{200}, crystalline peak) and the diffraction intensity at 2θ = 18° ($I_{2\theta\ 18°}$, amorphous phase valley). The data were obtained using XRD Commander software (Bruker AXS GmbH, Karlsruhe, Germany) and processed with DIFFRAC.EVA (Bruker AXS GmbH, Karlsruhe, Germany) and DRXWin (Windows, version 2.3) software.

$$CI\ (\%) = \frac{(I_{200} - I_{2\theta\ 18°})}{I_{200}} 100 \quad (1)$$

2.3.7. Thermogravimetric analysis

A TGA analyser (TGA 1 Stare System analyser, Mettler-Toledo, Switzerland) was used to analyse the thermal behaviour of the cellulosic samples under nitrogen atmosphere (10 mL.min^{-1}). Samples of about 3–4 mg were weighed in an alumina pan and heated from 25 to 700 °C. Before the analysis, the samples were conditioned in desiccators with P_2O_5 at 25 °C for 2 weeks. The thermogravimetric and their derivatives curves were analysed using the STARe Evaluation Software (Mettler-Toledo, Switzerland) to obtain the initial temperature (T_{onset}), the temperature at the maximum degradation rate (T_{peak}), and the mass loss percentage in each detected thermal event. The measurements were

Table 1
Mass fraction (g/g) of the different components (MC: methylcellulose; GA: gum Arabic; Gly: glycerol; CMF: cellulose microfibres) present in the composite films.

Formulations	X_{MC}	X_{GA}	X_{Gly}	X_{CMF}
Control	0.7500	0.0833	0.1667	–
USH-1	0.7438	0.0823	0.1653	0.0086
USH-3	0.7317	0.0813	0.1626	0.0244
USH-5	0.7200	0.0800	0.1600	0.0400
ALK-1	0.7438	0.0823	0.1653	0.0086
ALK-3	0.7317	0.0813	0.1626	0.0244
ALK-5	0.7200	0.0800	0.1600	0.0400

taken in triplicate.

2.4. Reinforcing capacity and effect on physical properties in composite films

To evaluate the reinforcing capacity of the obtained fibres, films of Methylcellulose (MC) and Gum Arabic (GA), a polysaccharide-protein complex fully compatible with MC polymer (Amalraj et al., 2020; Xu et al., 2019), were obtained and characterised, using different ratios (1, 3 and 5 wt% with respect to the total polymer mass) of cellulose fibres. These blends were chosen on the basis of the good fibre compatibility visually observed. Table 1 summarises the different composition of the obtained films. Aqueous dispersions of cellulose fibres at different concentrations were sonicated (Vibra Cell™ VCX750, 750 W power, 20 kHz frequency, Sonics & Material, United States) at 25 °C (using an ice bath) for 20 min for the purposes of obtaining the films. Afterwards, MC (6% wt.) was added to the sonicated aqueous dispersions of cellulose fibres at 85 ± 2 °C and 700 rpm for 1 h (solution 1). Solution 2 was prepared by dispersing GA (2% wt.) in distilled water at 50 ± 2 °C and 700 rpm for 1 h. After that, a volume of solution 2 was mixed with solution 1 to reach the MC:GA mass ratio of 9:1. Later on, glycerol (20% wt. with respect to the total polymer mass) was added, and the final solution was stirred at 50 ± 2 °C and 700 rpm for 1 h. The amount of dispersion equivalent to 2 g of MC/GA blend was poured onto 150 mm diameter Teflon plates and dried at 25 ± 2 °C for 72 h. The cast films were labelled as USH-1, USH-3, USH-5, ALK-1, ALK-3, ALK-5, where the number indicates the wt. percentage of CF in the films, with respect to the polymers and USH or ALK indicate the method used to obtain the cellulose fibre prior to the bleaching process. As control samples, fibre-free MC/GA blended films were used. Before the characterisation, the composite films were conditioned at 53% RH (using a $Mg(NO_3)_2$ over-saturated solution) for one week. The films were prepared in triplicate.

2.5. Film characterisation

The optical properties (transparency and colour) were analysed in composite films. A spectrocolorimeter (CM-3600d, Minolta Co., Japan) was used to determine the reflection spectra (R) of the films from 400 to 700 nm, obtained on white (R_g) and black (R_0) backgrounds. The internal transmittance (T_i) used to determine the transparency and the infinite reflectance (R_∞) were obtained, following the Kubelka-Munk theory of multiple scattering (Eqs. (2)–(5)). Film colour coordinates L^* (lightness), a^* (redness-greenness), and b^* (yellowness-blueness) were obtained from the R_∞ spectra, using D65 illuminant and 10° observer. Chroma (C^*) and hue angle (h^*) were obtained following Eqs. (6) and (7), respectively. The measurements were taken six times for each sample (Andrade, González-Martínez, & Chiralt, 2020).

$$T_i = \sqrt{(a + R_0)^2 - b^2} \tag{2}$$

$$R_\infty = a - b \tag{3}$$

$$a = \frac{1}{2}\left[R + \left(\frac{R_0 - R + R_g}{R_0 \times R_g}\right)\right] \tag{4}$$

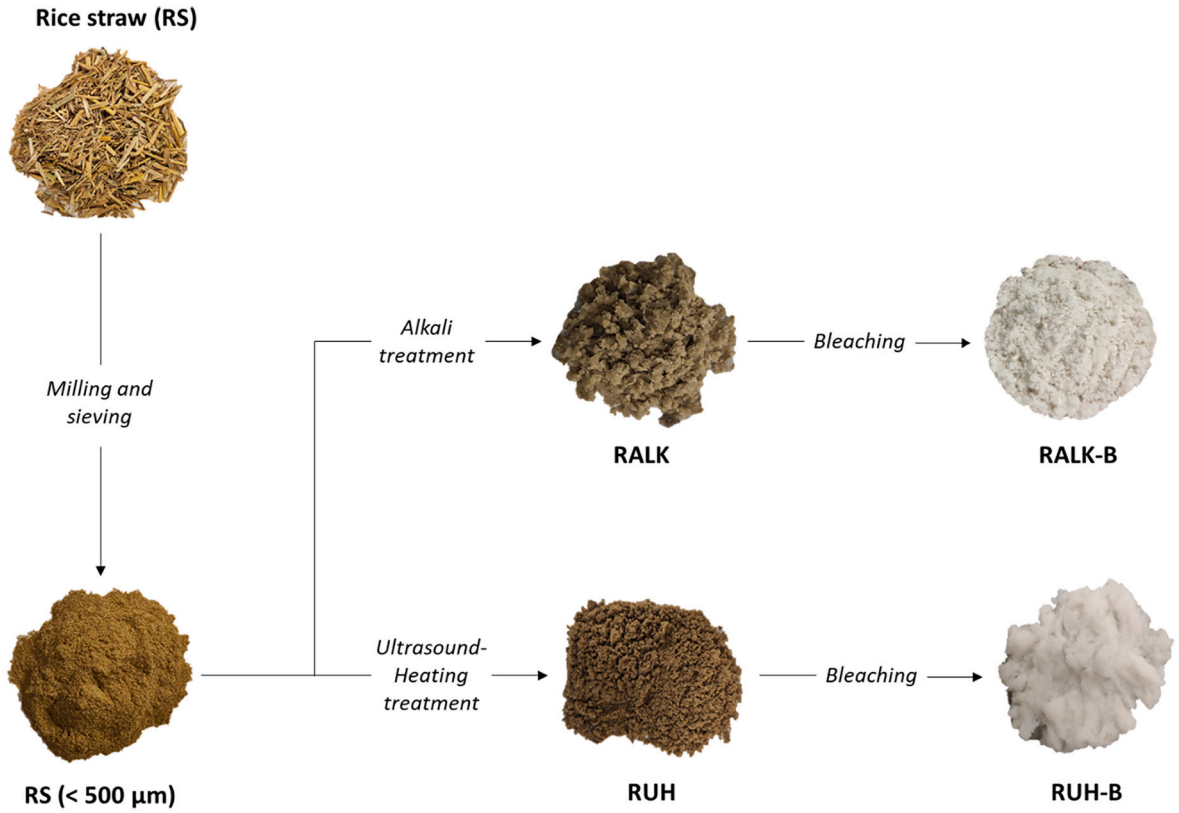

Fig. 1. Different fractions obtained in the cellulose extraction process by applying a combined US-heating process or alkaline treatment before the bleaching step.

Table 2
Yield, chemical composition (% wt.), and the ashes content of RS and the cellulosic fractions at different treatment steps (mean values ± standard deviation of three replicates).

Sample	Yield (% wt.)	Water extractables (% wt.)	Cellulose* (% wt.)	Hemicellulose* (% wt.)	Lignin (% wt.)	Ashes (% wt.)
RS	–	9.3 ± 0.8^{a}	36.7 ± 0.4^{e}	19.3 ± 0.1^{a}	21.2 ± 0.5^{a}	17 ± 2^{a}
RUS	85.5	12.3 ± 0.2^{b}	37.3 ± 0.1^{de}	21.3 ± 0.2^{a}	20.5 ± 0.2^{a}	12 ± 1^{b}
RUH	80.1	14.8 ± 0.1^{c}	40.3 ± 0.8^{d}	20.1 ± 1.2^{a}	19.7 ± 1.4^{a}	11 ± 1^{b}
RALK	31.2	n/a	54.6 ± 3.1^{c}	8.2 ± 1.2^{c}	6.6 ± 1.7^{b}	8 ± 1^{c}
RUH-B	37.4	n/a	65.9 ± 0.7^{b}	15.6 ± 0.4^{b}	5.2 ± 0.2^{b}	5 ± 2^{cd}
RALK-B	29.5	n/a	73.4 ± 2.1^{a}	10.1 ± 0.8^{c}	2.6 ± 0.4^{c}	2 ± 3^{d}

* Cellulose was reported as % wt. of total glucose content in relation to the initial solid fraction; hemicellulose concentration was determined by the sum of the xylose and arabinose contents.

$$b = \sqrt{a^2 - 1} \quad (5)$$

$$C^* = \sqrt{a^{*2} + b^{*2}} \quad (6)$$

$$h^* = arctg\left(\frac{b^*}{a^*}\right) \quad (7)$$

The water vapour permeability (WVP) of films, expressed in g.mm. kPa^{-1} h^{-1}.m^{-2}, was determined gravimetrically, following ASTM E96/E96M (ASTM, 2005) with a modification proposed by McHugh et al. (1993). The samples were cut and placed in circular cups (Ø = 3.5 cm) containing 5 mL of distilled water (100% RH). Then, the cups were put into desiccators at 25 °C and 53% RH ($Mg(NO_3)_2$ over-saturated solution), which promoted a constant RH gradient of 47% through the films. The systems were weighed every 1.5 h for 24 h, and the water vapour transmission rate was determined from the slope of the curve given by weight loss *vs.* time. The measurements were taken in triplicate.

The equilibrium water content of the films was determined gravimetrically following the method of Collazo-Bigliardi et al. (2019), with modifications. About 500 mg of each conditioned film (25 °C and 53% RH for one week) was dried at 60 °C for 24 h and then placed in a dissector at 25 °C with P_2O_5 for two weeks. The moisture content was obtained from the mass loss of the film samples. The measurements were taken in triplicate.

The thickness of films was measured using a digital micrometer (Palmer, model COMECTA, Barcelona, accuracy of 0.001 mm) at ten random film positions.

According to ASTM D882 (ASTM, 2012), a universal testing machine (Stable Micro Systems, TA.XT plus, England) was used to determine the tensile properties of the films. The force-distance curves were obtained and transformed into stress-Hencky strain curves. The mechanical behaviour was analysed in terms of elastic modulus (EM), tensile strength (TS) and percentage of elongation at break (%E). The pre-conditioned (53% RH) film samples (25 mm × 100 mm) were stretched at a crosshead speed of 12.5 $mm.min^{-1}$ by two grips initially separated by 50 mm. Eight samples for each treatment were evaluated in triplicate.

2.6. Statistical analysis

The experimental data were submitted to analysis of variance (ANOVA) using the Minitab statistical program (version 17), considering a confidence level of 95%. Differences between the responses of the treatments were determined by Tukey's studentised range (HSD) test, using the least significant difference (α) of 5%.

3. Results and discussion

3.1. Extraction and purification process of CF

Fig. 1 shows the appearance of the products obtained in each step of the processes used for obtaining CF from RS: the alkaline treatment and the sequential combination of ultrasounds and reflux heating of the RS aqueous dispersion, both followed by a bleaching step. The appearance of the RUH-B fibres (Fig. 1) suggests that the combined ultrasound-heating process was comparable to that performed with alkaline solution (RALK-B) since both products exhibited similar whiteness. The untreated RS particles and the cellulosic fractions were characterised as to their chemical composition, nano and microstructural characteristics and thermostability. The reinforcing capacity of cellulosic fibres was evaluated once incorporated into MC polymeric films.

Table 2 summarizes the yield (referred to the initial dry RS) of the different solid fractions from each stage of obtaining process of the cellulose fibres, as well as water extractables and the chemical composition of raw RS and different fractions. The lower yields obtained at each stage (31.2% and 29.5% for RALK and RALK-B, respectively) suggested that the alkaline method was more effective at extracting non-cellulosic compounds than the RUH treatment, with greater yields in the insoluble material (85.5%, 80.1% and 37.4% for RUS, RUH, and RUH-B, respectively). Thus, the alkaline process seems to promote greater tissue degradation with higher removal of hemicellulose, lignin, and waxes from RS (Faruk, 2012; Jones, Ormondroyd, Curling, Popescu, & Popescu, 2017; Pickering, Efendy, & Le, 2016), giving rise to a more purified cellulosic fraction. This was confirmed by the chemical composition analyses. The untreated RS showed cellulose, hemicellulose, and lignin contents of 36.7%, 19.3%, and 21.2%, respectively, consistent with the values found by Singh, Tiwari, Srivastava, and Shukla (2014). A progressive enrichment in cellulose content was observed for both treatments, according to the elimination of non-cellulosic components present in the raw RS. However, the samples submitted to the alkaline step (RALK-B) exhibited higher cellulose content and lower hemicellulose and lignin concentrations than those obtained by applying the combined ultrasound-heating method (RUH-B). Ultrasound (RUS) treatment step and combined method (RUH) only produced a slight, non-significant ($p > 0.5$), decrease in the lignin content of the solid fraction while the hemicellulose content slightly increased due to the removal of other water soluble compounds. However, the cellulose concentrations in the final fibres obtained from both purification methods (alkaline and combined treatment) were more comparable after the bleaching step (73% *vs.* 66%, respectively). This result suggests that the main effect of the combined method was to disrupt the tissues of the RS, exposing the innermost tissue of the plant matrix, thus favouring the contact with the bleaching solvent. This is also coherent with the higher values of water extractables of RUS and RUH samples, compared with the raw RS sample. The extraction potential of the non-structural, water-soluble components from the solid plant tissue was promoted by RUS and RUH treatments (Table 2). Acoustic cavitation promoted by ultrasound is characterised by the implosion or explosion of water vapour or air bubbles, which generates high shear rates in the solvent (Ojha, 2020). This phenomenon transfers high amounts of energy to the dispersed material, causing the plant cell to rupture and extracting non-cellulosic compounds (Arruda, 2019; Cheung & Wu, 2013). Thus, US exposes tissues of the plant matrix and, when used in combination with heating, can increase the mass transfer efficiency. Freitas et al. (2020) observed that ultrasound promoted debonding in the RS fibrils, which increased the surface area of the plant

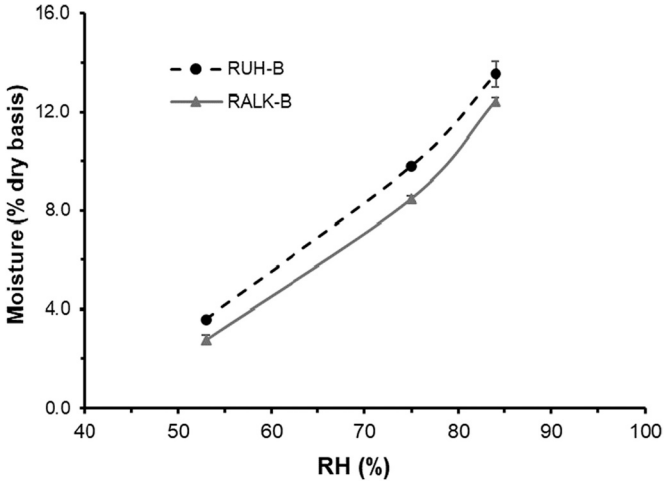

Fig. 2. Equilibrium moisture content (% wt. dry basis) at 25 °C at different relative humidity of the cellulose fibres obtained by applying the combined ultrasound-heating method (RUH-B) and the alkaline treatment (RALK-B).

material exposed to the extraction medium. These physical changes allowed greater accessibility of the solvent when the heating step was applied, enhancing the extraction levels of components, such as hemicelluloses, lignin, or waxes.

RS showed an ash content of approximately 17% wt., which is mainly attributed to silica (Chen, 2011). The subsequent purification steps promoted a progressive reduction in the ash/silica content, suggesting the leaching out of these non-carbonaceous components. The fractions submitted to the alkaline treatment showed a lower ash content (RALK: 7.5%) than those RUH treated (11%) since the alkaline solution promoted the solubility of silica (Requena et al., 2019). Bleaching promoted the silica extraction from the lignocellulosic residue in both RALK and RUH solids, but its final content was higher in cellulosic fractions obtained by the combined RUH treatment.

As concerns the water binding capacity of the fibres, Fig. 2 shows the equilibrium water content of RALK-B and RUH-B fibres at different relative humidity. Significantly lower values were obtained for the RALK-B samples, which suggests the presence of a higher amount of exposed polar groups in the cellulosic materials coming from RUH-B treatment that promoted the fibre water affinity. This could be attributed to the higher purification of the cellulose chains in the RALK-B samples, which contributes to exposing the cellulosic OH groups that are able to establish hydrogen bonds between chains. The extensive hydrogen bonding between the cellulose chains decreases their capacity to interact/bond with water molecules (Bochek, 2003), thus reducing the hydrophilic nature of the fibre.

3.2. Structural properties

The micro and nanostructural properties of the different cellulosic fractions were evaluated as to their microscopic characteristics, particle size distribution, FTIR analysis, and X-ray diffraction patterns. Fig. 3

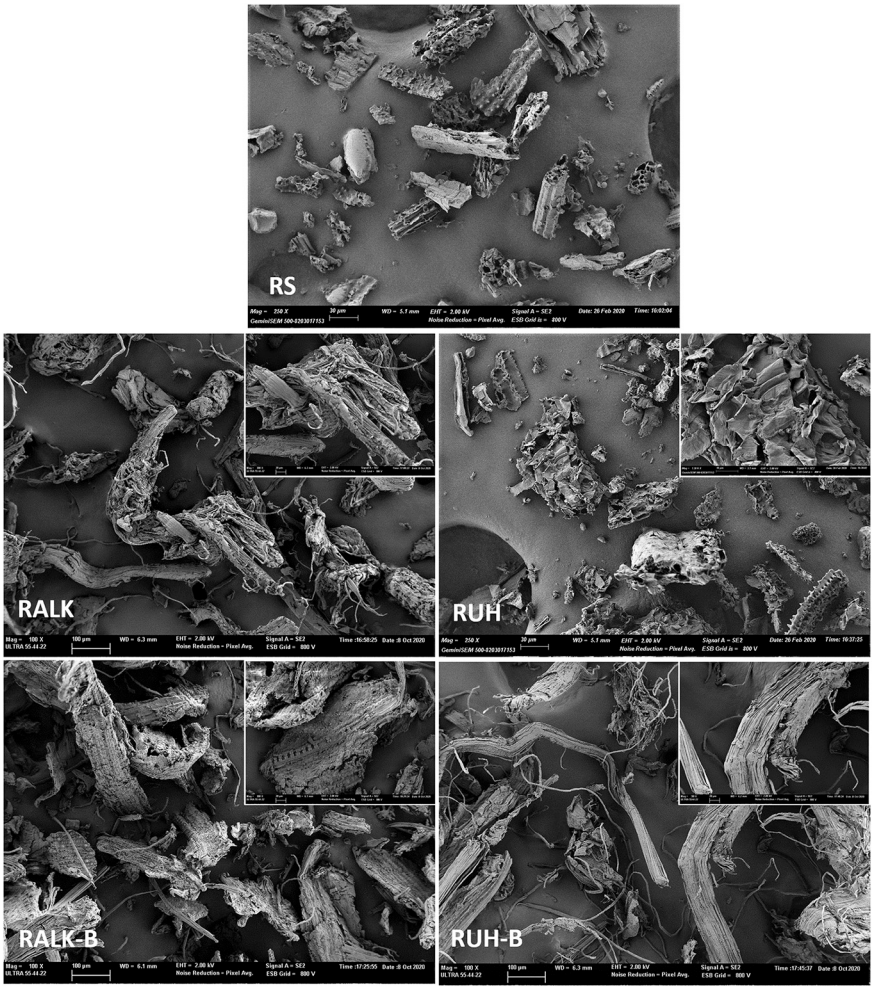

Fig. 3. FESEM micrographs of cellulosic fractions before and after the bleaching step, in comparison with raw material (RS).

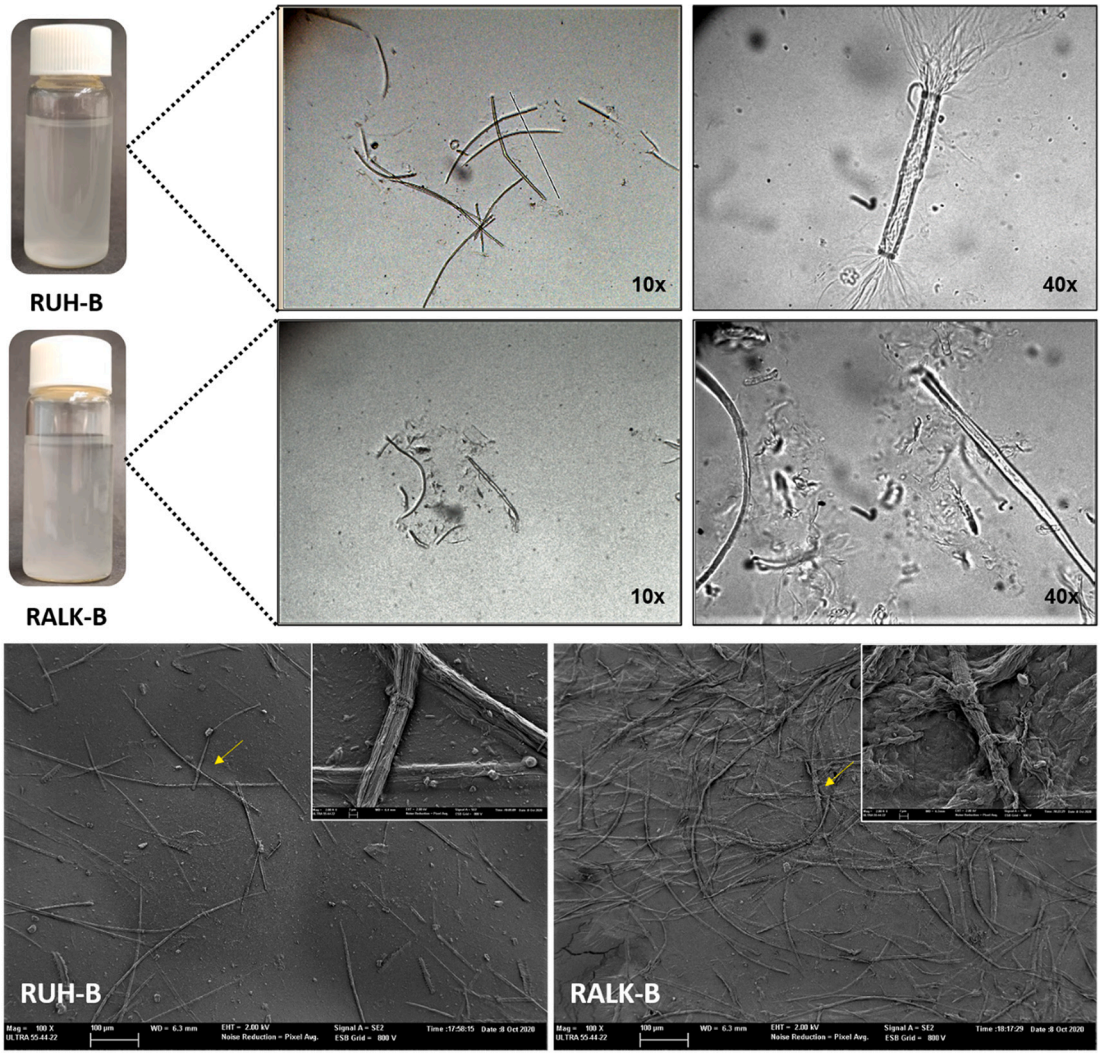

Fig. 4. Optical and FESEM micrographs of the CF (RUH-B and RALK-B) sonicated aqueous dispersions before and after drying, respectively.

shows the FESEM micrographs in which the microstructural changes in the RS provoked by the CF extraction can be observed. The raw sample (RS) exhibited particles of different dimensions and sizes obtained after the milling and sieving steps. The predominantly fibrillar rod-like shape of the particles reveals the RS tissue arrangement, which consists of a material with a high proportion of non-fibrous cells, such as the epidermis, parenchyma, and vessel cells (Jin & Chen, 2006). The innermost primary tissue, namely the sclerenchyma, is composed of CF embedded in a cementing matrix of hemicellulose and lignin (Seo & Sakoda, 2014). As shown in the micrograph of the RUH treated samples, the application of ultrasound followed by heating provoked the partial destruction of the original RS structures brought about by the different physical phenomena involved, such as detexturation, sonoporation and particle fragmentation (Chemat, 2017; Machado, 2019; Ojha, 2020). The RS tissue layers were observed to detach, leading to distorted and more planar particles, thus favouring the leaching out of non-cellulosic components, such as hemicellulose, lignin, and waxes. The observed disruption of the original RS structure facilitates the accessibility of the bleaching solvent to the solid matrix. It is worth mentioning that the removal of non-fibrous components from the cellulosic material was not evident at this stage. In contrast, the FESEM images from the RALK treated samples showed more intact particles than those RUH treated, despite being more distorted longitudinally, as also observed by (Moslemi, 2020). The observation of fibres aligned in the axial direction suggests the partial chemical removal of amorphous components, such as hemicellulose, lignin, and waxes (Zhang et al., 2014). This effect was more evident for RALK-B and RUH-B treated samples, which revealed smooth and homogeneous surface patterns due to an efficient surface washing of non-fibrous components, as also reported by other authors for the extraction of different plant matrices (Mohamad Haafiz, Eichhorn, Hassan, & Jawaid, 2013; Rasheed, Jawaid, Karim, & Abdullah, 2020). A certain degree of defibrillation was detected for the RUH-B samples at the edges of the fibre bundles (Fig. 4), which suggests that the ultrasound-heating treatment disrupted the fibre bundle structure to a greater extent than the alkaline treatment.

Fig. 4 shows optical microscopy and FESEM observations of the CF obtained from RUH-B and RALK-B treatments after their aqueous dispersions and sonication for 20 min, before and after drying, respectively. Before drying, optical micrographs (10× magnification) revealed that the original fibre bundles were disrupted, and the defibrillated fibre bundles of varying lengths were dispersed in the aqueous medium, increasing the turbidity and dispersion consistency. At a greater magnification (40× magnification), detached cellulose fibrils can be observed at the edges of the fibres in the RUH-B samples (black arrows) but not in the samples treated with alkaline solution (RALK-B). This could be due to the effect of the alkaline treatment, which could eliminate these defibrillated fractions, or to the greater weakness of the fibril unions in the bundle provoked by the RUH treatment. These variations in the fibre structure could also affect the hydrophilic nature of the different fibres, as demonstrated by the different equilibrium water

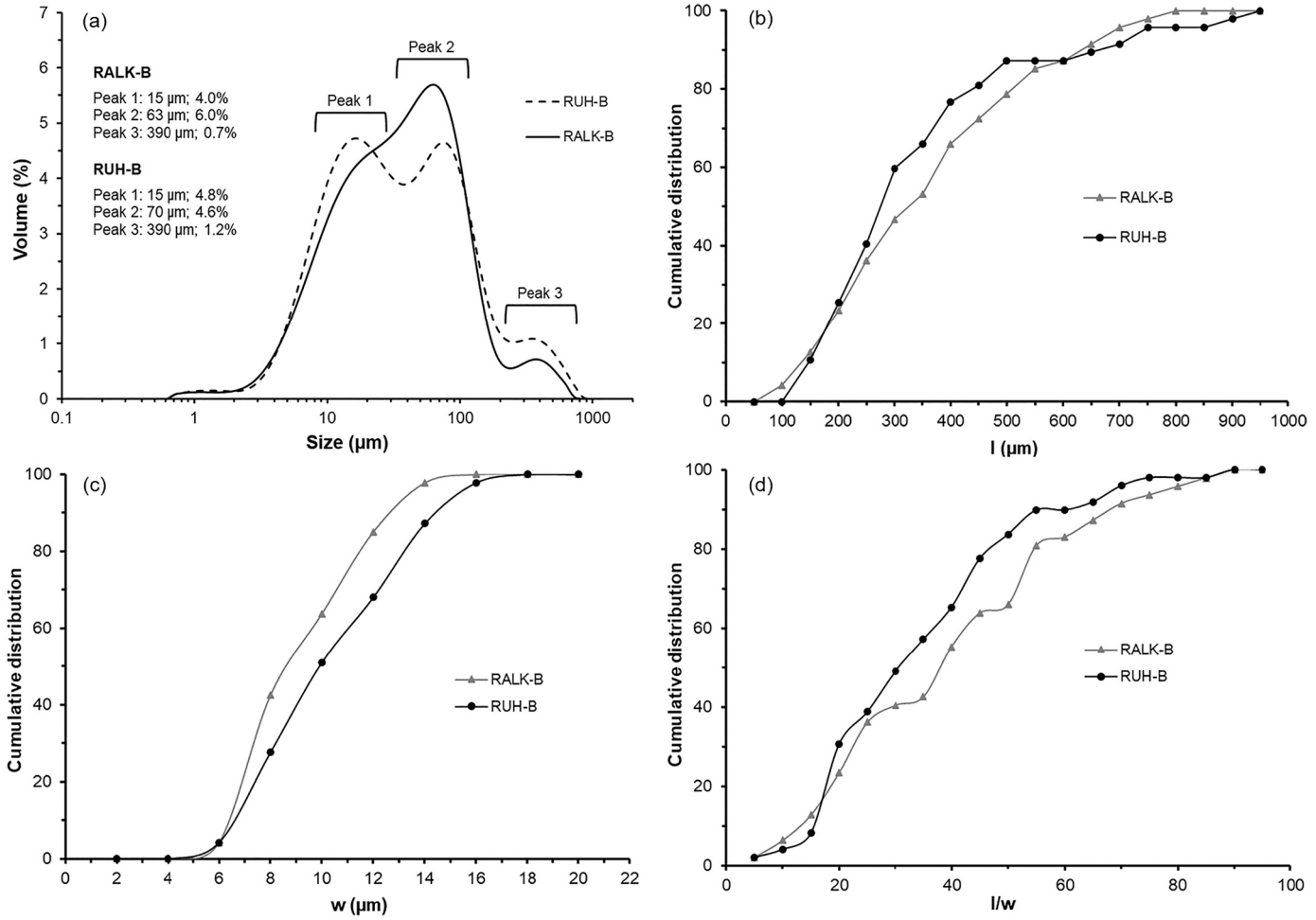

Fig. 5. Particle size distributions of CF from laser diffraction (a) and cumulative distributions of CF (RALK-B and RUH-B) samples obtained from the image analyses of optical microscopy images (b: length (l); c: width (w); d: aspect ratio (l/w)).

content. In this sense, the alkaline treatment removes more compounds from the lignocellulosic fibre, promoting hydrogen bonds between cellulose chains, further reducing the interaction capacity with water molecules. What is remarkable is the large number of small fibre fragments, together with the largest fibres, in the RALK-B sample, which suggest the more aggressive effect of the alkaline treatment on the fibrous material. After drying the sonicated aqueous dispersions of fibres, the FESEM micrographs reveal that the fibres of the RUH-B treated samples remained mostly isolated, whereas those of the RALK-B treated samples exhibited aggregation with fibre entanglement. This reveals the different interaction forces between the two kinds of fibres, probably due to the different number of OH groups exposed on their surface due to the differences in the degree of cellulose purification. Greater attractive forces acted between the more hydrophobic RALK-B fibres, whereas repulsive interactions acted on the more hydrophilic RUH-B materials. These results ratify the different nature of the fibre's surface (more or less hydrophilic), as affected by the kind of treatment.

Laser diffraction was also used to investigate the morphogeometric properties of CF in terms of particle size distributions derived from their hydrodynamic volume. As can be observed in Fig. 5a, the RUH-B and RALK-B samples exhibited an almost bimodal distribution, with two main peaks at about 15 and 70 μm. The RUH-B samples have a greater ratio of small particles (4.8% volume fraction) than the RALK-B samples (4%). So, the RUH treatment provoked a greater fraction of smaller particles (around 15 μm), or less aggregated particles, in comparison with the alkaline treatment. Nevertheless, it is remarkable that laser diffraction measurements provide the radius of gyration of the particles and so, the values are closer to the particle length. In this sense, the RALK-B treatment could give rise to longer fibres than the RUH-B, which could be due, in part, to the defibrillation effect observed at the edges of the fibrils (Fig. 4).

Considering the CF rod-like shape, image analysis was applied to the optical micrographs in order to determine the cumulative distribution of the length (l), width (w), and the aspect ratio (l/w) of the CF (RUH-B and RALK-B) after water dispersion by sonication (Fig. 4b, c, and d). A similar length distribution can be observed for the different particles, the maximum frequency being for fractions of lengths of 200–350 μm. Nevertheless, as detected in laser diffraction analyses, a greater ratio of shorter particles can be observed for the RUH-B treatment, whereas the RALK-B particles exhibited a wider length distribution. In contrast, a remarkable reduction in the particle width may be observed for the sonicated fibres, which had values of under 20 μm (Fig. 5c), as also shown in the FESEM images at a higher magnification (Fig. 4). A greater fraction of thinner particles can be observed for the RALK-B samples; more than 60% of the particles are thinner than 10 μm. This is coherent with the fact that the alkaline treatment removes a greater quantity of non-cellulosic components from the fibre. Consequently, the aspect ratio (l/w) of the RALK-B samples is slightly greater than that of the RUH-B samples, with a distribution ranging mainly between 10 and 50 (RUH-B) or 60 (RALK-B) (Fig. 5d).

3.3. Fourier transform infrared spectroscopy (FTIR)

Fig. 6 shows the FTIR spectra of untreated RS and unbleached (RUH

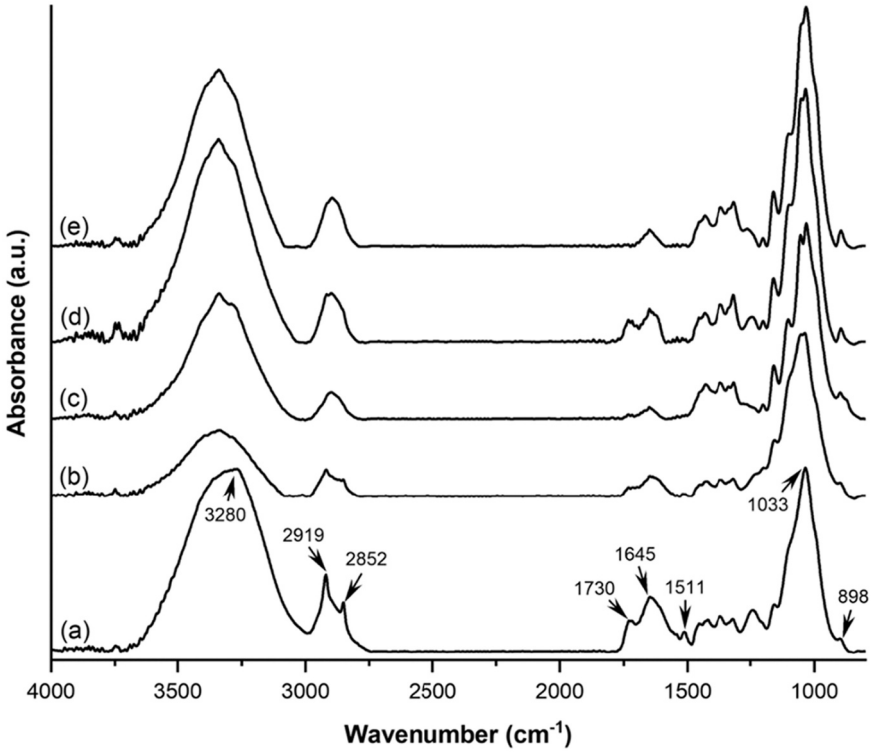

Fig. 6. FTIR spectra of (a) untreated RS, RS treated with (b) ultrasound-heating and (c) alkaline solution, and bleached fibres from (d) the combined ultrasound-heating method and (e) the alkaline treatment.

and RALK) and bleached (RUH-B and RALK-B) cellulosic fractions. The spectrum of untreated RS showed a bell-shaped absorption band between 3690 and 2980 cm^{-1}, which is associated with the O—H stretching vibration (Chen, 2011). The O—H absorption band, present in cellulose, hemicellulose, and lignin, was slightly narrower and more intense for the bleached samples. This agrees with the cellulose concentration in the material (Table 2) since it has a higher ratio of OH groups than non-cellulosic components (hemicellulose and lignin) (Moslemi, 2020; Wang, 2018). The absorption bands at 2919 and 2852 cm^{-1} are associated with the C-H asymmetric and symmetrical vibration present in cellulose, hemicellulose, and lignin. These peaks shared more characteristics in RS and RUH treated samples, indicating a more similar composition, whereas there were greater differences between the both bleached samples (RUH-B and RALK-B), according to the greater elimination of non-cellulosic compounds by alkaline treatment. The absorption peak at 1730 cm^{-1} corresponds to the C═O stretching vibration of the carboxylic groups and esters present in phenolic and uronic acids, which are chemical structures constituting the lignin and hemicellulose fractions (Abraham, 2011; Chen, 2011). This peak disappeared partially in the RALK treated samples and totally in the RALK-B treated samples. However, it was present in the spectra of the bleached and non-bleached RUH treated samples, which indicates the presence of these kinds of compounds bonded to the cellulose structure, according to the chemical composition (Table 2). Wang (2018) also observed the disappearance of this peak after the alkaline treatment of rice straw, whereas (Boonterm, 2016) detected the peak at 1730 cm^{-1} in cellulose obtained with the thermal steam explosion from rice straw. The different intensities of the bands at 1645 cm^{-1}, assigned to the O-H bending vibration of adsorbed water (Moslemi, 2020), coincides with the differences in the equilibrium moisture content of the samples; the samples coming from the RUH treatments exhibiting the higher intensity. Indeed, Chen (2011) indicated that the lower intensity of this peak is related to a partial removal of hemicellulose. The thin peak at 1511 cm^{-1} corresponds to the C═C stretching vibration of the aromatic skeletons present in lignin rings (Elhussieny, 2020; Xu et al., 2006). This

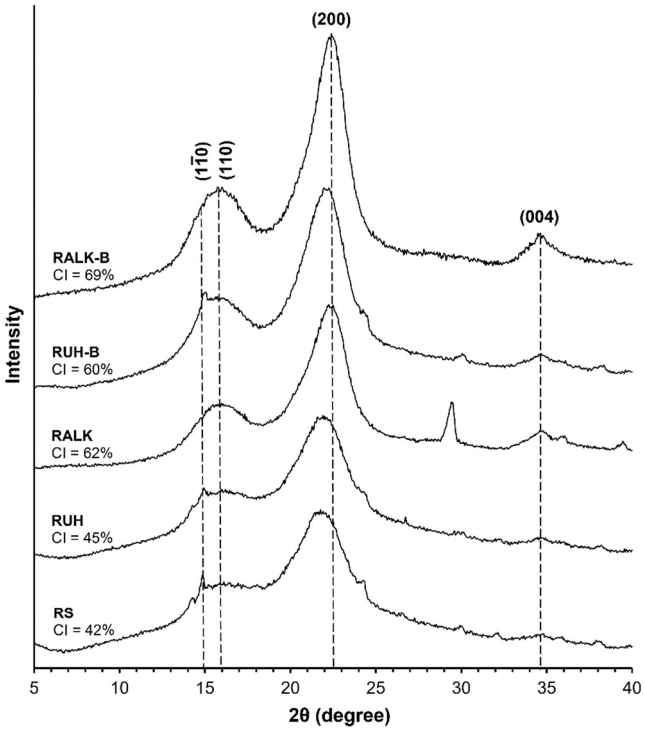

Fig. 7. The X-ray diffractograms and crystallinity index (CI) of different cellulosic fractions from RS, before and after bleaching.

absorption band is absent in the spectra of the RALK treated samples and every bleached sample (RUH-B and RALK-B), thus indicating the efficiency of bleaching at eliminating a substantial fraction of lignin. Every spectrum showed an absorption band at 1033 cm^{-1}, related to the

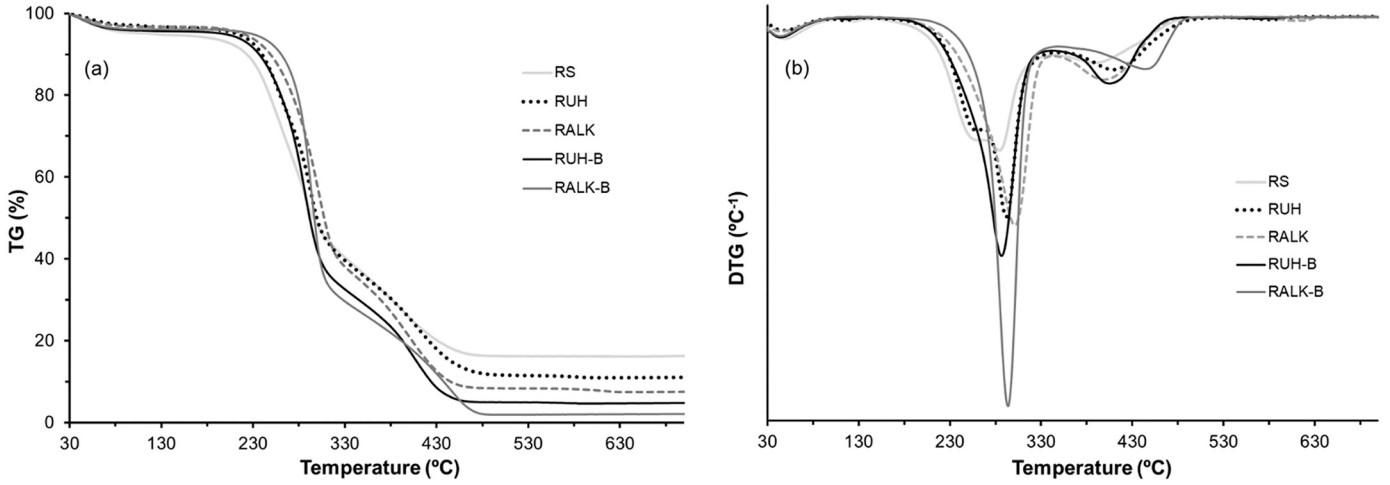

Fig. 8. The TGA (a) and DTGA (b) curves of the RS samples before and after different treatments: RUH, RALK, RUH-B, and RALK-B.

C—O—C—O—C stretching vibration of acetal linkage present in cellulose and hemicellulose. The 898 cm^{-1} band, associated with the C—O—C stretching vibration of the β-glycosidic bond present in the cellulose I structure, becomes more evident as the cellulose concentration increases in the bleached samples (RALK-B and RUH-B) (Pan & Sano, 2005; Wang, 2018). In brief, the obtained FTIR spectra suggested that, despite the alkaline method eliminating a greater fraction of hemicellulose and lignin from the plant matrix, the combined ultrasound-heating treatment produced similar fibres and could be alternatively applied to RS as a greener process.

3.4. Crystallinity analysis

The X-ray diffraction patterns of the raw powder and the different cellulosic fractions obtained at each stage of both processes are shown in Fig. 7. Likewise, the crystalline nature of the materials was characterised in terms of the crystallinity index (CI). In every sample, four diffraction peaks were detected at $2\theta = 15^{\circ}$ ($1\bar{1}0$), 16° (110), 22° (200), and 34° (004), characteristic of the crystalline lattice of type I cellulose, as described by other authors (Junior, 2018; Nam, French, Condon, & Concha, 2016). As the cellulose purification progressed, the diffraction peaks became more defined and slightly narrower, as corresponds to the progressive elimination of amorphous components (hemicellulose, lignin, and waxes). Compared to RS (CI: 42%), the combined ultrasound-heating method (RUH) promoted a negligible increase in crystallinity (CI: 45%), whereas a noticeable increase was observed for the cellulosic sample after the treatment with alkaline solution (CI: 62%), similar to that obtained by Requena et al. (2019) for rice husk treated with alkaline solution. This agrees with what was deduced from chemical composition and FTIR analyses; the combined ultrasound-heating method was less efficient at extracting amorphous components from the plant matrix than the alkaline treatment. In addition to the chemical degradation and removal of amorphous components from the lignocellulosic matrix, NaOH solutions at low concentrations promote the swelling of interfibrillar regions, making them less rigid (Liu & Hu, 2009; Yue et al., 2012). This phenomenon allows for the rearrangement of the cellulose microfibrils, due to the penetration of Na ions into the crystalline network forming antiparallel crystalline soda-cellulose complexes, which change the crystallinity of the material (Budtova & Navard, 2016; Liu & Hu, 2009). From a determined NaOH concentration (e.g., 15% for cotton fibre), a crystalline transition can occur, giving rise to the formation of cellulose II crystals (Yue et al., 2012). This change was not clearly observed in the RS samples treated with the alkaline solution due to the low NaOH concentration used (4.5%).

After the bleaching step, which focuses on removing lignin from the matrix (Ng et al., 2015b; Zainuddin, 2013), CI increased in both samples, but especially in the RUH-B samples. This suggests that, despite the ultrasound-heating combined method failing to eliminate a substantial fraction of lignin/hemicellulose components, the fibre delamination and the greater exposure of the RS tissue, observed by FESEM, seem to promote the bleaching solvent accessibility (Freitas et al., 2020). Thus, this produces cellulosic materials with similar crystalline characteristics to those produced by the conventional alkaline method, but containing other bonded compounds as revealed by chemical composition and FTIR analyses.

3.5. Thermogravimetric analysis

The thermal behaviour of the samples as the extraction progressed was evaluated by thermogravimetric analysis (TGA). Both the TGA and the derivative (DTGA) curves of the untreated, different cellulosic fractions are shown in Fig. 8. Table 3 summarises the parameters (initial and maximum degradation temperatures and the mass loss percentage) of each detected thermal event. Each cellulosic sample exhibited three thermal degradation events. The first occurred in the temperature range of 30 to 140 °C, associated with the loss of water molecules bonded on cellulosic fractions and other small molecular weight volatiles (Theng et al., 2017; Wu, Yao, Xu, Mei, & Zhou, 2013). The second and third peaks are related to the thermal degradation of the lignocellulosic components, as reported by other authors (Requena et al., 2019). As can

Table 3
Thermal decomposition events detected for the cellulosic materials from RS (mean values ± standard deviation of two replicates).

Sample	[30–140] °C			[148–350] °C			[340–500] °C			Residue
	T_{onset}*	T_{peak}*	Mass loss (%)	T_{onset}*	T_{peak}*	Mass loss (%)	T_{onset}*	T_{peak}*	Mass loss (%)	Mass (%)
RS	33.19 ± 0.01	51.4 ± 2.0	1.7 ± 0.2	148 ± 5	284.2 ± 0.2	55.9 ± 1.5	345.5 ± 2.1	389 ± 2	20.7 ± 0.6	17 ± 2
RALK	33.0 ± 1.7	49.9 ± 1.5	0.9 ± 0.1	161 ± 1	301.3 ± 2.4	61.0 ± 2.2	341.7 ± 1.1	403 ± 7	26.8 ± 0.2	8 ± 1
RUH	32.3 ± 0.6	50.5 ± 1.3	1.2 ± 0.2	152 ± 2	292.4 ± 2.2	59.7 ± 0.9	349.0 ± 1.7	409 ± 3	23.8 ± 0.4	11 ± 1
RALK-B	33.7 ± 2.1	47.9 ± 2.1	1.1 ± 0.2	186 ± 7	294.0 ± 4.0	69.0 ± 7.0	349.0 ± 3.0	448 ± 8	24.0 ± 1.2	2 ± 3
RUH-B	33.3 ± 0.6	47.1 ± 2.3	1.3 ± 0.6	177 ± 2	286.0 ± 4.0	66.3 ± 2.3	344.0 ± 3.0	414 ± 15	27.0 ± 5.0	5 ± 2

Table 4
Moisture content, WVP, and mechanical properties of the MC/GA blended films with or without different ratios of CMF from RS (mean values ± standard deviation of three replicates for moisture content and WVP; and eight replicates for thickness and mechanical parameters).

Formulation	Moisture (%)	*WVP** (x10^3) (g.mm. kPa^{-1} h^{-1}. m^{-2})	Thickness (μm)	EB* (%)	TS* (MPa)	EM* (MPa)
Control	9.8 ± 0.4^{a}	4.3 ± 0.2^{ab}	119 ± 8^{c}	9.1 ± 2.1^{e}	23.0 ± 3.0^{c}	156 ± 13^{a}
USH-1	8.8 ± 0.4^{bc}	4.2 ± 0.2^{ab}	121 ± 5^{bc}	13.7 ± 2.2^{bcd}	28.1 ± 1.2^{a}	161 ± 6^{a}
USH-3	8.0 ± 0.3^{cd}	4.3 ± 0.1^{ab}	129 ± 7^{ab}	12.0 ± 0.8^{cde}	28.0 ± 2.0^{a}	156 ± 13^{a}
USH-5	7.6 ± 0.4^{d}	4.6 ± 0.3^{a}	133 ± 8^{a}	11.8 ± 1.9^{de}	28.3 ± 1.4^{a}	152 ± 15^{a}
ALK-1	8.8 ± 0.3^{bc}	4.5 ± 0.3^{a}	127 ± 7^{abc}	16.1 ± 2.2^{ab}	27.0 ± 4.0^{ab}	157 ± 17^{a}
ALK-3	8.5 ± 0.4^{cd}	4.2 ± 0.2^{ab}	126 ± 4^{abc}	16.7 ± 2.1^{a}	24.2 ± 2.2^{bc}	127 ± 16^{b}
ALK-5	9.5 ± 0.2^{ab}	3.9 ± 0.1^{b}	124 ± 4^{bc}	14.7 ± 1.8^{ab}	24.2 ± 2.1^{bc}	122 ± 14^{b}

Different letters in the same column indicate significant differences by the Tukey test (α = 0.05).
* *WVP*: water vapour permeability; EB: elongation at break; TS: tensile strength at break; EM: elastic modulus.

be observed, the second thermal event started at higher temperatures as the cellulose became more purified, in the following order: RS < RUH < RALK<RUH-B < RALK-B. The peak temperature ranged between 284 and 300 °C, depending on the sample. This agrees with the fact that the RALK/RUH and bleaching treatments eliminated hemicellulosic/lignin fractions to differing extents, as observed by the chemical composition, FTIR and XRD analyses, increasing the sample degradation temperature. The peak observed in the DTGA curve of the RALK-B sample was narrower and more intense than that of the RUH-B sample, in line with the greater purity and crystallinity of the cellulose fraction.

On the other hand, lignin is a group of polymers that exhibits a broad spectrum of thermal degradation starting at around 220 °C and continuing above 400 °C (Monteiro, Calado, Margem, & Rodriguez, 2012). In this sense, as reported by Theng et al. (2017), the last thermal event, observed between at 340–500 °C is attributed to the thermal degradation of the lignin and the products from the fragmentation of the organic structure. This peak, also found by El-Sakhawy and Hassan (2007) in microcrystalline cellulose from RS, was not expected in the thermograms of bleached fibres, which indicates the inability of either process to eliminate completely the lignin present in the inner structure of the fibre bundles. Indeed, the FESEM images (Fig. 3) reveal some integral and compact fibre bundles, which could prevent the full access of the bleaching solvent. According to Chen (2011), the strong crystalline structure of cellulose in RS and the complexity of the structural configuration between cellulose, hemicellulose, and lignin are the limiting factors for the obtaining of accessible cellulose fibres.

3.6. Reinforcing properties in composite CMC/GA films

The reinforcement capacity of fibres obtained by means of the alternative (ultrasound-heating) and conventional (alkaline) methods was evaluated by measuring the tensile properties of MC/GA composite films incorporating different fibre ratios. The use of GA, a polysaccharide-protein complex (Maqbool, 2011; Xu et al., 2019), as a component of the MC polymer matrix was chosen to promote the compound compatibility, since GA exhibits excellent surfactant and encapsulating properties with other polymers and compounds (Amalraj et al., 2020; Xu et al., 2018). The reinforced capacity transfer from the CF to the polymer matrix is related to factors such as the microfibre entanglement, the intensity and type of microfibre-polymer interactions and the ratio between the water adsorption (which promotes plasticisation) and the filler rigidity. Thus, the mechanical properties of the composite films containing the different types and concentrations of CF were evaluated in terms of their tensile strength (TS) and elongation at break (%EB), as well as the elastic modulus (EM) (Table 4). In general, all of the composite films became mechanically more resistant to break and stretchable (p < 0.05) after CF incorporation (greater TS and %EB values). So, films with 1% and 3% of RALK-B fibres exhibited a 77%

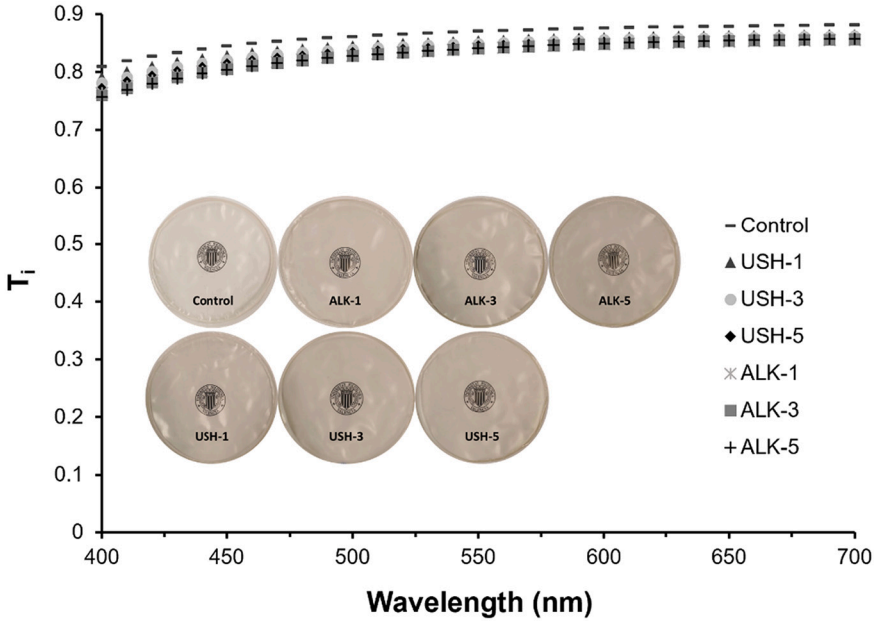

Fig. 9. Internal transmittance of the MC/GA blended films with different types (RUH-B and RALK-B) and concentrations (0%, 1%, 3%, and 5% wt.) of CF.

increase in EB, while the treatments incorporating RUH-B fibres in the same concentrations increased extensibility by about 33%. The incorporation of a greater amount of fibres (5%) reduced film stretchability, compared with the lower ratios. Cazón, Vázquez, and Velazquez (2018) also reported an increase in the stretchability for the films based on PVA/chitosan with 5% microcrystalline cellulose. As shown in Fig. 4, the RUH-B and RALK-B exhibited high aspect ratios, which enhanced the entanglement, interfacial interaction, and bondability between the cellulose microfibrils and the MC/GA matrix (Littunen, Hippi, Saarinen, & Seppälä, 2013; Ng et al., 2015b). Thus, CF incorporation promoted the force transferring from the microfibril to the polymer matrix. Nevertheless, a non-significant increase ($p > 0.05$) in the EM values was observed for the CF reinforced films, as observed by other authors for cellulose acetate films with cellulose nanofibers from RS (Hassan et al., 2019). Even elastic modulus was reduced by about 20% when 3 or 5% of the CF from the ALK treatment was incorporated into the films. As concerns the resistance to break of the films (TS), CF from the RUH treatments increased the TS values by about 22% at every tested ratio, whereas this effect was only observed in fibres from the ALK treatment at 1%. Therefore, both kinds of fibres exhibited a reinforcing effect on the MC/GA films, which was reflected in different patterns: the RUH fibres promoted the film resistance to break to a greater extent, but were less effective at enhancing the film stretchability, whereas the RALK fibres made the films more stretchable. Likewise, 5% of CF did not benefit the film tensile behaviour more than 1–3%.

Table 4 also summarises the thickness, moisture content values and water vapour permeability (WVP) of the studied films. The equilibrium moisture content of the films decreased as the CF ratio rose, although 5% of RALK fibres did not provoke this effect. The OH groups present in the cellulose microfibrils could interact with hydrophilic groups within the MC-GA-glycerol matrix, making these sites less available to interact with water molecules. Nevertheless, the lower water content of the films with CF did not lead to lower values of film thickness. In fact, the thickness of the films did not significantly change as a result of fibre addition, except when RUH fibres were incorporated at 3 and 5%, in which case the films were slightly thicker, according to the increase in the surface solid density of the films. As concerns the WVP values, fibre addition only provoked a significant decrease (about 10%) when obtained by means of the ALK treatment and incorporated at 5%. Therefore, despite the expected increase in the tortuosity factor for mass transfer promoted by fibres, no improvement in the water barrier capacity of the films was obtained probably due to the hydrophilic nature of these fibres that favours water solubility in the matrix. Other authors have also found no improvement in the water vapour barrier capacity of the films when CF were incorporated into polymer matrices (Azmin, Hayat, Binti, & Nor, 2020; Cazón et al., 2018; Collazo-Bigliardi et al., 2019).

Fig. 9 shows the appearance and the internal transmittance spectra of MC/GA-based films with different fibres and ratios. All of the composite films were similar in appearance to the control film, indicating good compatibility and entanglement of the CF in the polymer matrix. This was reflected in the small changes that occurred in the internal transmittance spectra (Fig. 7) of the different samples provoked by fibre addition. As the fibre concentration rose, there was a slight decrease in the transparency of the films, due to the negligible light scattering effect provoked by the CF dispersion in the polymer matrix, as also observed by other authors (Ching et al., 2015).

4. Conclusions

Although alkaline treatment is the most common step in the process for obtaining CF, its substitution by an ultrasound-heating method has environmental advantages due to the elimination of alkaline solvents. This new method gave rise to cellulose fibre fractions with a slightly different degree of purification, but with a similar degree of crystallinity and aspect ratio, these being more hydrophilic in nature and with a lower tendency to aggregate. The reinforcing capacity of the fibres obtained with this new method was similar to those obtained using the alkaline treatment, enhancing the film stretchability by about 33%, and boosting the film resistance to break (by about 20%) at 1, 3 or 5%.

Therefore, the combined ultrasound-heating method can be a potential alternative for the purposes of obtaining CF from RS, avoiding the use alkaline solutions, is faster and presents a higher yield than the process with an alkaline step (37 *vs.* 29%). Moreover, the ultrasound-heating method allows for obtaining active extracts rich in antioxidant compounds, which can be used for different applications in the food or pharmaceutical industries. Thus, a more integral valorisation of RS could be reached.

Funding

This work was supported by Generalitat Valenciana for the GrisoliaP/2019/115 Grant.

Declaration of Competing Interest

The authors have no conflict of interest to declare.

Acknowledgments

P.A.V.F. is grateful to Generalitat Valenciana for the GrisoliaP/2019/115 grant. We also thank María del Sol Juan Borras (Institute of Food Engineering for Development), Universitat Politècnica de València for her assistance with chemical composition analysis.

References

Abraham, E. (2011). Extraction of nanocellulose fibrils from lignocellulosic fibres: A novel approach. *Carbohydrate Polymers, 8*.

Amalraj, A., Haponiuk, J. T., Thomas, S., & Gopi, S. (2020). Preparation, characterization and antimicrobial activity of polyvinyl alcohol/gum arabic/chitosan composite films incorporated with black pepper essential oil and ginger essential oil. *International Journal of Biological Macromolecules, 151*, 366–375. https://doi.org/10.1016/j.ijbiomac.2020.02.176

Andrade, J., González-Martínez, C., & Chiralt, A. (2020). The incorporation of carvacrol into Poly (vinyl alcohol) films encapsulated in lecithin liposomes. *Polymers, 12*(2), 497. https://doi.org/10.3390/polym12020497

Arruda, H. S. (2019). *Effects of high-intensity ultrasound process parameters on the phenolic compounds recovery from araticum peel* (p. 14).

ASTM. (2005), *2005. Standard Test Methods for Water Vapor Transmission of Materials, E96/E96M, 2005* (pp. 1–11). American Society for Testing and Materials. Annual Book of ASTM Standards, C.

ASTM. (2012). ASTM. Standard test method for tensile properties of thin plastic sheeting. In , *D882-12, Vol. 12,. ASTM*. American Society for Testing and Materials.

Azmin, S. N. H. M., Hayat, N. A., Binti, M., & Nor, M. S. M. (2020). Development and characterization of food packaging bioplastic film from cocoa pod husk cellulose incorporated with sugarcane bagasse fibre. *Journal of Bioresources and Bioproducts, 5*(4), 248–255. https://doi.org/10.1016/j.jobab.2020.10.003

Barana, D., Salanti, A., Orlandi, M., Ali, D. S., & Zoia, L. (2016). Biorefinery process for the simultaneous recovery of lignin, hemicelluloses, cellulose nanocrystals and silica from rice husk and Arundo donax. *Industrial Crops and Products, 86*, 31–39. https://doi.org/10.1016/j.indcrop.2016.03.029

Bochek, A. M. (2003). Effect of hydrogen bonding on cellulose solubility in aqueous and nonaqueous solvents. *Russian Journal of Applied Chemistry, 76*(11), 1711–1719. https://doi.org/10.1023/B:RJAC.0000018669.88546.56

Boonterm, M. (2016). Characterization and comparison of cellulose fiber extraction from rice straw by chemical treatment and thermal steam explosion. *Journal of Cleaner Production, 8*.

Budtova, T., & Navard, P. (2016). *Cellulose in NaOH-water based solvents: A review* (p. 105).

Casabar, J. T., Ramaraj, R., Tipnee, S., & Unpaprom, Y. (2020). Enhancement of hydrolysis with Trichoderma harzianum for bioethanol production of sonicated pineapple fruit peel. *Fuel, 279*, 118437. https://doi.org/10.1016/j.fuel.2020.118437

Cazón, P., Vázquez, M., & Velazquez, G. (2018). Novel composite films based on cellulose reinforced with chitosan and polyvinyl alcohol: Effect on mechanical properties and water vapour permeability. *Polymer Testing, 69*, 536–544. https://doi.org/10.1016/j.polymertesting.2018.06.016

Chemat, F. (2017). Ultrasound assisted extraction of food and natural products. Mechanisms, techniques, combinations, protocols and applications. A review. *Ultrasonics Sonochemistry*, 21.

Chen, X. (2011). Study on structure and thermal stability properties of cellulose fibers from rice straw. *Carbohydrate Polymers, 6*.

Cheung, Y.-C., & Wu, J.-Y. (2013). Kinetic models and process parameters for ultrasound-assisted extraction of water-soluble components and polysaccharides from a

medicinal fungus. *Biochemical Engineering Journal, 79*, 214–220. https://doi.org/10.1016/j.bej.2013.08.009
Ching, Y. C., Rahman, A., Ching, K. Y., Sukiman, N. L., & Cheng, H. C. (2015). Preparation and characterization of polyvinyl alcohol-based composite reinforced with nanocellulose and nanosilica. *BioResources, 10*(2), 3364–3377. https://doi.org/10.15376/biores.10.2.3364-3377
Collazo-Bigliardi, S. (2018). Isolation and characterisation of microcrystalline cellulose and cellulose nanocrystals from coffee husk and comparative study with rice husk. *Carbohydrate Polymers, 11*.
Collazo-Bigliardi, S., Ortega-Toro, R., & Chiralt, A. (2019). Improving properties of thermoplastic starch films by incorporating active extracts and cellulose fibres isolated from rice or coffee husk. *Food Packaging and Shelf Life, 22*, 100383. https://doi.org/10.1016/j.fpsl.2019.100383
Elhussieny, A. (2020). Valorisation of shrimp and rice straw waste into food packaging applications. *Ain Shams Engineering Journal, 8*.
El-Sakhawy, M., & Hassan, M. L. (2007). Physical and mechanical properties of microcrystalline cellulose prepared from agricultural residues. *Carbohydrate Polymers*, 10.
FAOSTAT. (2018). Recuperado 4 de noviembre de 2020, de. http://www.fao.org/faostat/en/#data/QC/visualize.
Faruk, O. (2012). Biocomposites reinforced with natural fibers: 2000–2010. *Progress in Polymer Science*, 45.
Freitas, P. A. V., González-Martínez, C., & Chiralt, A. (2020). Application of ultrasound pre-treatment for enhancing extraction of bioactive compounds from rice straw. *Foods, 9*(11), 1657. https://doi.org/10.3390/foods9111657
Harini, K., & Chandra Mohan, C. (2020). Isolation and characterization of micro and nanocrystalline cellulose fibers from the walnut shell, corncob and sugarcane bagasse. *International Journal of Biological Macromolecules, 163*, 1375–1383. https://doi.org/10.1016/j.ijbiomac.2020.07.239
Hassan, M., Berglund, L., Abou-Zeid, R., Hassan, E., Abou-Elseoud, W., & Oksman, K. (2019). Nanocomposite film based on cellulose acetate and lignin-rich rice straw nanofibers. *Materials, 12*(4), 595. https://doi.org/10.3390/ma12040595
Ilyas, R. A., Sapuan, S. M., Ibrahim, R., Abral, H., Ishak, M. R., Zainudin, E. S., … Jumaidin, R. (2019). Effect of sugar palm nanofibrillated cellulose concentrations on morphological, mechanical and physical properties of biodegradable films based on agro-waste sugar palm (Arenga pinnata (Wurmb.) Merr) starch. *Journal of Materials Research and Technology, 8*(5), 4819–4830. https://doi.org/10.1016/j.jmrt.2019.08.028
Jin, S., & Chen, H. (2006). Structural properties and enzymatic hydrolysis of rice straw. *Process Biochemistry, 4*.
Jones, D., Ormondroyd, G. O., Curling, S. F., Popescu, C.-M., & Popescu, M.-C. (2017). Chemical compositions of natural fibres. In *Advanced high strength natural fibre composites in construction* (pp. 23–58). Elsevier. https://doi.org/10.1016/B978-0-08-100411-1.00002-9.
Junior, M. G. (2018). *Effect of the nano-fibrillation of bamboo pulp on the thermal, structural, mechanical and physical properties of nanocomposites based on starch/poly(vinyl alcohol) blend* (p. 27).
Kargarzadeh, H. (2017). Starch biocomposite film reinforced by multiscale rice husk fiber. *Composites Science and Technology*, 9.
Kassab, Z. (2020). Cellulosic materials from pea (*Pisum Sativum*) and broad beans (*Vicia Faba*) pods agro-industrial residues. *Materials Letters, 4*.
Kimura, T., Sakamoto, T., Leveque, J.-M., Sohmiya, H., Fujita, M., Ikeda, S., & Ando, T. (1996). Standardization of ultrasonic power for sonochemical reaction. *Ultrasonics Sonochemistry, 3*(3), S157–S161. https://doi.org/10.1016/S1350-4177(96)00021-1
Korotkova, E., Pranovich, A., Wärnå, J., Salmi, T., Murzin, D. Y., & Willför, S. (2015). Lignin isolation from spruce wood with low concentration aqueous alkali at high temperature and pressure: Influence of hot-water pre-extraction. *Green Chemistry, 17*(11), 5058–5068. https://doi.org/10.1039/C5GC01341K
Littunen, K., Hippi, U., Saarinen, T., & Seppälä, J. (2013). Network formation of nanofibrillated cellulose in solution blended poly(methyl methacrylate) composites. *Carbohydrate Polymers, 91*(1), 183–190. https://doi.org/10.1016/j.carbpol.2012.08.032
Liu, Y., & Hu, H. (2009). *X-ray diffraction study of bamboo fibers treated with NaOH* (p. 5).
Machado, I. (2019). *Characterization of the effects involved in ultrasound-assisted extraction of trace elements from artichoke leaves and soybean seeds* (p. 7).
Maqbool, M. (2011). Postharvest application of gum arabic and essential oils for controlling anthracnose and quality of banana and papaya during cold storage. *Postharvest Biology and Technology, 6*.
McHugh, T. H., Avena-Bustillos, R., & Krochta, J. M. (1993). Hydrophilic Edible Films: Modified Procedure for Water Vapor Permeability and Explanation of Thickness Effects. *Journal of Food Science, 58*, 899–903.
Menzel, C., González-Martínez, C., Vilaplana, F., Diretto, G., & Chiralt, A. (2020). Incorporation of natural antioxidants from rice straw into renewable starch films. *International Journal of Biological Macromolecules, 146*, 976–986. https://doi.org/10.1016/j.ijbiomac.2019.09.222
Mohamad Haafiz, M. K., Eichhorn, S. J., Hassan, A., & Jawaid, M. (2013). Isolation and characterization of microcrystalline cellulose from oil palm biomass residue. *Carbohydrate Polymers, 93*(2), 628–634. https://doi.org/10.1016/j.carbpol.2013.01.035
Monteiro, S. N., Calado, V., Margem, F. M., & Rodriguez, R. J. S. (2012). Thermogravimetric stability behavior of less common lignocellulosic fibers—A review. *Journal of Materials Research and Technology, 1*(3), 189–199. https://doi.org/10.1016/S2238-7854(12)70032-7
Moslemi, A. (2020). Addition of cellulose nanofibers extracted from rice straw to urea formaldehyde resin; effect on the adhesive characteristics and medium density fiberboard properties. *International Journal of Adhesion and Adhesives*, 6.
Nam, S., French, A. D., Condon, B. D., & Concha, M. (2016). Segal crystallinity index revisited by the simulation of X-ray diffraction patterns of cotton cellulose Iβ and cellulose II. *Carbohydrate Polymers, 135*, 1–9. https://doi.org/10.1016/j.carbpol.2015.08.035
Ng, H.-M., Sin, L. T., Tee, T.-T., Bee, S.-T., Hui, D., Low, C.-Y., & Rahmat, A. R. (2015a). Extraction of cellulose nanocrystals from plant sources for application as reinforcing agent in polymers. *Composites Part B: Engineering, 75*, 176–200. https://doi.org/10.1016/j.compositesb.2015.01.008
Ng, H.-M., Sin, L. T., Tee, T.-T., Bee, S.-T., Hui, D., Low, C.-Y., & Rahmat, A. R. (2015b). Extraction of cellulose nanocrystals from plant sources for application as reinforcing agent in polymers. *Composites Part B: Engineering, 75*, 176–200. https://doi.org/10.1016/j.compositesb.2015.01.008
Nunes, M. R., de Souza Maguerroski Castilho, M., de Lima Veeck, A. P., da Rosa, C. G., Noronha, C. M., Maciel, M. V. O. B., & Barreto, P. M. (2018). Antioxidant and antimicrobial methylcellulose films containing *Lippia alba* extract and silver nanoparticles. *Carbohydrate Polymers, 192*, 37–43. https://doi.org/10.1016/j.carbpol.2018.03.014
Ojha, K. S. (2020). Ultrasound technology for the extraction of biologically active molecules from plant, animal and marine sources. *Trends in Analytical Chemistry, 10*.
Pan, X., & Sano, Y. (2005). Fractionation of wheat straw by atmospheric acetic acid process. *Bioresource Technology, 96*(11), 1256–1263. https://doi.org/10.1016/j.biortech.2004.10.018
Peanparkdee, M., & Iwamoto, S. (2019). Bioactive compounds from by-products of rice cultivation and rice processing: Extraction and application in the food and pharmaceutical industries. *Trends in Food Science & Technology, 86*, 109–117. https://doi.org/10.1016/j.tifs.2019.02.041
Pickering, K. L., Efendy, M. G. A., & Le, T. M. (2016). A review of recent developments in natural fibre composites and their mechanical performance. *Composites Part A: Applied Science and Manufacturing, 83*, 98–112. https://doi.org/10.1016/j.compositesa.2015.08.038
Prakash, A., Vadivel, V., Banu, S. F., Nithyanand, P., Lalitha, C., & Brindha, P. (2018). Evaluation of antioxidant and antimicrobial properties of solvent extracts of agro-food by-products (cashew nut shell, coconut shell and groundnut hull). *Agriculture and Natural Resources, 52*(5), 451–459. https://doi.org/10.1016/j.anres.2018.10.018
Rasheed, M., Jawaid, M., Karim, Z., & Abdullah, L. C. (2020). *Morphological, physiochemical and thermal properties of microcrystalline cellulose (MCC) extracted from bamboo fiber* (p. 15).
Requena, R., Jiménez-Quero, A., Vargas, M., Moriana, R., Chiralt, A., & Vilaplana, F. (2019). Integral fractionation of rice husks into bioactive arabinoxylans, cellulose nanocrystals, and silica particles. *ACS Sustainable Chemistry & Engineering, 7*(6), 6275–6286. https://doi.org/10.1021/acssuschemeng.8b06692
Saha, S., & Ghosh, R. (2019). Cellulose nanocrystals from lignocellulosic agro-waste: A comparative study on conventional and ultrasonic assisted preparation methods. *Materials Today: Proceedings, 11*, 628–636. https://doi.org/10.1016/j.matpr.2019.03.020
Saini, J. K., Saini, R., & Tewari, L. (2015). Lignocellulosic agriculture wastes as biomass feedstocks for second-generation bioethanol production: Concepts and recent developments. *3. Biotech, 5*(4), 337–353. https://doi.org/10.1007/s13205-014-0246-5
Salam, A., Reddy, N., & Yang, Y. (2007). Bleaching of kenaf and cornhusk fibers. *Industrial & Engineering Chemistry Research, 46*(5), 1452–1458. https://doi.org/10.1021/ie061371c
Sarkar, N., Ghosh, S. K., Bannerjee, S., & Aikat, K. (2012). Bioethanol production from agricultural wastes: An overview. *Renewable Energy, 37*(1), 19–27. https://doi.org/10.1016/j.renene.2011.06.045
Segal, L., Creely, J. J., & Martin, A. E. (1959). An Empirical Method for Estimating the Degree of Crystallinity of Native Cellulose Using the X-Ray Diffractometer. *Textile research journal, 29*(10), 786–794.
Seo, D.-J., & Sakoda, A. (2014). Assessment of the structural factors controlling the enzymatic saccharification of rice straw cellulose. *Biomass and Bioenergy, 71*, 47–57. https://doi.org/10.1016/j.biombioe.2014.10.027
Sharma, B., Vaish, B., Monika, Singh, U. K., Singh, P., & Singh, R. P. (2019). Recycling of organic wastes in agriculture: An environmental perspective. *International Journal of Environmental Research, 13*(2), 409–429. https://doi.org/10.1007/s41742-019-00175-y
Singh, R., Tiwari, S., Srivastava, M., & Shukla, A. (2014). Microwave assisted alkali pretreatment of rice straw for enhancing enzymatic digestibility. *Journal of Energy, 2014*, 1–7. https://doi.org/10.1155/2014/483813
Sluiter, A. (2008a). *Determination of extractives in biomass: Laboratory analytical procedure (LAP)* (issue date 7/17/2005. Technical Report, 12).
Sluiter, A. (2008b). *Determination of structural carbohydrates and lignin in biomass: Laboratory analytical procedure (LAP)* (issue date: April 2008; revision date: July 2011 (Version 07-08-2011). Technical Report, 18).
Sumere, B. R., de Souza, M. C., dos Santos, M. P., Bezerra, R. M. N., da Cunha, D. T., Martinez, J., & Rostagno, M. A. (2018). Combining pressurized liquids with ultrasound to improve the extraction of phenolic compounds from pomegranate peel (*Punica granatum* L.). *Ultrasonics Sonochemistry, 48*, 151–162. https://doi.org/10.1016/j.ultsonch.2018.05.028
Takano, M., & Hoshino, K. (2018). Bioethanol production from rice straw by simultaneous saccharification and fermentation with statistical optimized cellulase cocktail and fermenting fungus. *Bioresources and Bioprocessing, 5*(1), 16. https://doi.org/10.1186/s40643-018-0203-y
Theng, D., Arbat, G., Delgado-Aguilar, M., Ngo, B., Labonne, L., Evon, P., & Mutjé, P. (2017). Comparison between two different pretreatment technologies of rice straw fibers prior to fiberboard manufacturing: Twin-screw extrusion and digestion plus

defibration. *Industrial Crops and Products, 107*, 184–197. https://doi.org/10.1016/j.indcrop.2017.05.049

Wang, Z. (2018). Rice straw cellulose nanofibrils reinforced poly(vinyl alcohol) composite films. *Carbohydrate Polymers*, 9.

Wanyo, P., Meeso, N., & Siriamornpun, S. (2014). Effects of different treatments on the antioxidant properties and phenolic compounds of rice bran and rice husk. *Food Chemistry, 157*, 457–463. https://doi.org/10.1016/j.foodchem.2014.02.061

Wu, Q., Yao, F., Xu, X., Mei, C., & Zhou, D. (2013). Thermal degradation of rice straw fibers: Global kinetic modeling with isothermal thermogravimetric analysis. *Journal of Industrial and Engineering Chemistry, 19*(2), 670–676. https://doi.org/10.1016/j.jiec.2012.10.026

Xu, F., Liu, C. F., Geng, Z. C., Sun, J. X., Sun, R. C., Hei, B. H., … Je, J. (2006). Characterisation of degraded organosolv hemicelluloses from wheat straw. *Polymer Degradation and Stability, 91*(8), 1880–1886. https://doi.org/10.1016/j.polymdegradstab. 2005.11.002

Xu, T., Gao, C., Feng, X., Yang, Y., Shen, X., & Tang, X. (2019). Structure, physical and antioxidant properties of chitosan-gum arabic edible films incorporated with cinnamon essential oil. *International Journal of Biological Macromolecules*, 7.

Xu, T., Gao, C., Yang, Y., Shen, X., Huang, M., Liu, S., & Tang, X. (2018). Retention and release properties of cinnamon essential oil in antimicrobial films based on chitosan and gum arabic. *Food Hydrocolloids, 84*, 84–92. https://doi.org/10.1016/j.foodhyd.2018.06.003

Xu, Y. (2013). Feasibility of nanocrystalline cellulose production by endoglucanase treatment of natural bast fibers. *Industrial Crops and Products, 4*.

Yue, Y., Zhou, C., French, A. D., Xia, G., Han, G., Wang, Q., & Wu, Q. (2012). Comparative properties of cellulose nano-crystals from native and mercerized cotton fibers. *Cellulose, 19*(4), 1173–1187. https://doi.org/10.1007/s10570-012-9714-4

Zainuddin, S. Y. Z. (2013). Potential of using multiscale kenaf fibers as reinforcing filler in cassava starch-kenaf biocomposites. *Carbohydrate Polymers, 7*.

Zhang, Z., Smith, C., & Li, W. (2014). Extraction and modification technology of arabinoxylans from cereal by-products: A critical review. *Food Research International*, 14.